LAWRENCE
LIVERMORE
NATIONAL
LABORATORY

UCRL-PROC-210861

Actinic inspection of multilayer defects on EUV masks

A. Barty, Y. Liu, E. Gullikson, J. S. Taylor, O. Wood

March 25, 2005

SPIE Microlithogrraphy
San Jose, CA, United States
August 2, 2005 through April 3, 2005

Actinic inspection of multilayer defects on EUV masks

Anton Barty[1], Yanwei Liu[2], Eric Gullikson[2], John S. Taylor[1] and Obert Wood[3]

[1] Lawrence Livermore National Laboratory, P.O. Box 808, Livermore, CA 94550
[2] Center for X-ray Optics, Lawrence Berkeley National Laboratory, 1 Cyclotron Road, Berkeley, CA 94720
[3] SEMATECH, 255 Fuller Road, Suite 309, Albany, NY 12203

The production of defect-free mask blanks, and the development of techniques for inspecting and qualifying EUV mask blanks, remains a key challenge for EUV lithography. In order to ensure a reliable supply of defect-free mask blanks, it is necessary to develop techniques to reliably and accurately detect defects on un-patterned mask blanks. These inspection tools must be able to accurately detect all critical defects whilst simultaneously having the minimum possible false-positive detection rate.

There continues to be improvement in high-speed non-actinic mask blank inspection tools, and it is anticipated that these tools can and will be used by industry to qualify EUV mask blanks. However, the outstanding question remains one of validating that non-actinic inspection techniques are capable of detecting all printable EUV defects.

To qualify the performance of non-actinic inspection tools, a unique dual-mode EUV mask inspection system has been installed at the Advanced Light Source (ALS) synchrotron at Lawrence Berkeley National Laboratory. In high-speed inspection mode, whole mask blanks are scanned for defects using 13.5-nm wavelength light to identify and map all locations on the mask that scatter a significant amount of EUV light. In imaging, or defect review mode, a zone plate is placed in the reflected beam path to image a region of interest onto a CCD detector with an effective resolution on the mask of 100-nm or better. Combining the capabilities of the two inspection tools into one system provides the unique capability to determine the coordinates of native defects that can be used to compare actinic defect inspection with visible light defect inspection tools under commercial development, and to provide data for comparing scattering models for EUV mask defects.

Keywords: extreme ultraviolet lithography; mask; reticle; defect;.

1 Multilayer defect inspection requirements

A typical EUV multilayer coating consists of 40-80 bilayers of molybdenum and amorphous silicon with each bilayer consisting of approximately 3nm Mo and 4nm Si. The reflectivity of the multilayer is a resonant property of the alternating layer structure and is at an optimum when all the layers interfere constructively; because reflection takes place throughout the bulk of the multilayer. Any deformation or disruption of the layer structure can manifest itself as a defect. Ideally the goal is to produce defect-free mask blanks; however this may be difficult to achieve in practice. It is therefore essential to have strategies for inspecting mask blanks prior to patterning in order to determine whether there are any defects present on the mask blank. It is anticipated that high-throughput visible light inspection tools will be used for this purpose in a production environment; however the defects are only critical if they manifest themselves in the EUV image at the wafer plane and meet a condition for "printability"[1]. It is necessary to determine whether there are any defects visible in the EUV that are not being detected by the visible light inspection tools in order to have confidence in the visible light inspection strategy. The purpose of the actinic inspection tool is to help answer this question.

[1] An anomaly observed on the mask during inspection is considered a defect if it is printable on the wafer and will likely affect the performance of the printed circuit per a standardized set of critera. Similarly, anomalies that are detected during inspection may not strictly be defects if they are not printable on the wafer or cause no unacceptable errors. For ease of discussion within this paper, all anomalies that are detected by an inspection tool are considered defects, and will be differentiated as printable or non-printable based on a subsequent review process, such as with the imaging mode of the present instrument.

The key requirement for a high-speed mask blank inspection system is to be able to capture all classes of printable mask defects. In practice this means that any mask that passes inspection will have an acceptably low probability of having a printable EUV defect that was not captured during inspection. Secondly it is desirable to be able to differentiate between printable and unprintable defects so as to minimize the number of masks wrongly rejected due to false positive counts. The problem of false positive and false negative counts is illustrated in Table 1:

		Printable defect	
		Defect	**No defect**
Non-actinic inspection result	**Defect**	Inspection is correct (desired result)	False positive (mask is actually OK)
	No defect	False Negative (defect exists but is not found)	Inspection is correct (desired result)

Table 1

The goal of non-actinic inspection is to obtain accurate discrimination between printable and non-printable defects based on non-EUV mask inspection. Both false positives and false negatives are undesirable, defined as a false determination of whether a given defect is likely to be a 'critical defect' for device function when printed in a lithographic tool.

One of the key risks for the commercial introduction of EUVL is that the non-actinic inspection systems will have false negatives, resulting in mask blanks that are erroneously classified as defect free. False negative defects are invisible to non-actinic inspection systems, but appear when the mask is imaged using EUV light. The premise behind the construction of the current instrument is that such defects can be detected using an EUV inspection system to inspect the multilayer structure. The key purpose of comparing EUV and non-EUV inspection systems is to determine the rate at which false positives and false negatives appear in commercial mask inspection systems based on non-EUV inspection technologies. An adjunct strategy is to verify the conclusions of the inspection comparison studies with actual printing in resist using an exposure tool, although that approach carries a much higher overhead, particularly with respect to the unknown presence and locations of native defects.

If non-actinic inspection alone is to be used for mask blank qualification, the non-actinic tool must correctly identify printable EUV defects on the mask blank with a high degree of confidence: Both false positives and false negatives affect mask cost of ownership in different ways:

1. False negatives: A non-actinic inspection tool that is not sensitive enough to capture all printable EUV defects is highly costly as it leads to defects that may only be discovered during or after patterning of the mask. Both the added cost involved invested in the patterning process, and the interruption to production once a defect is identified, make false negatives highly undesirable. It also makes identifying the source of the defect difficult as there is inherent uncertainty as to whether the defect was introduced during blank manufacture or during patterning. Due to the high cost of discovering defects at this stage of mask blank manufacture, we work with the assumption that the acceptable rate for false negatives counts is effectively 0%.

2. Correctly tuned: A non-actinic inspection tool that only detects printable EUV defects and does not result in any false positives or false negatives is clearly ideal, however may be difficult to achieve in practice. This is the ultimate goal for a fast non-actinic mask blank scanning system.

3. False positives: A non-actinic inspection tool that is oversensitive will record false positives by wrongly classifying features (anomalies) that do not print at EUV wavelengths as defects. If no actinic mask blank

review tool is used, the capture of false positives directly affects yield through the rejection of otherwise useable mask blanks. The acceptable rate of false positives is dependent on the mask cost model, but given the anticipated high cost of implementing actinic mask inspection into the production flow we assume that a small number of false positives will be acceptable provided the false positive counts do not lower mask blank yield by more than 10%.

Of the above options having a tool with the right sensitivity is clearly the preferred option; however this may be difficult to achieve in practice. For example, the different surface topography of multilayer defects means that EUV scattering and defect printability may not necessarily be completely correlated with the signal measured in a non-actinic inspection tool. The overall goal of implementing high-speed actinic mask inspection is to assist in the development of high-speed non-actinic inspection systems by determining the correlation, if any, between defect printability and the signal observed a non-actinic inspection tool. These three heads of mask inspection – actinic inspection, non-actinic inspection and defect printability can be arranged and interlinked as shown in Figure 1:

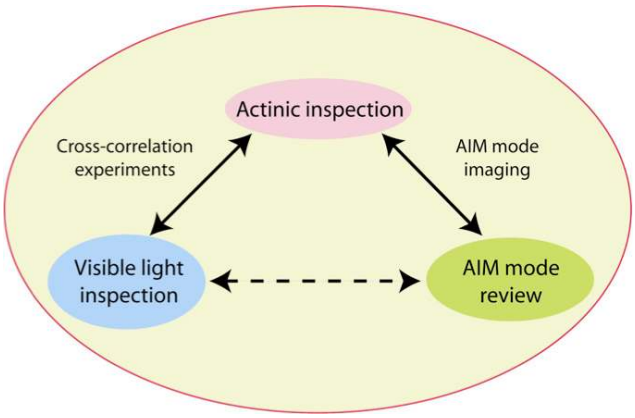

Figure 1

The three heads of mask blank inspection. Ideally one would want to form the correlation between the visible light inspection signal and defect printability as measured in a defect review tool. High-speed actinic inspection helps form this link by providing access to both actinic defect inspection and aerial image mode defect review in the one tool.

Ideally a correlation could be formed between defect printability and the signal observed a non-actinic inspection tool – the dashed line in Figure 1. This could be done directly by either printing large areas of patterned masks in a printing tool and searching the printed pattern for defects, or by inspecting large areas of a mask blank with an at-wavelength defect review microscope[2] or reticle inspection microscope[3]. Such schemes are currently impractical to implement in practice, particularly for masks that do not consist of known 'programmed' defects. Inspection of printing results using patterned masks is time consuming and does not differentiate adequately between patterning defects and multilayer defects, whilst reviewing large areas of mask blank with an actinic microscope would be a time-consuming proposition.

The actinic inspection tool helps bridge this gap by first scanning the mask at high-speed to detect variations in the EUV reflection from a mask blank looking for the at-wavelength signature of a defect. This ensures that even defects invisible to non-actinic inspection methods but visible in the EUV are registered. Once a defect is located the inspection tool revisits the defects in AIM mode to determine the defect printability. By comparing the result obtained using both the EUV and non-actinic inspection tools on the same defects it is possible to study the correlation between defect printability and the defect signature in a non-actinic inspection tool.

---

[2] A.Barty, J.S.Taylor, R.Hudyma, E.Spiller, D.W.Sweeney, G.Shelden and J-P Urbach, "Aerial image microscopes for the inspection of defects in EUV masks" (2002) 1889 Proc. SPIE 1073.

[3] A. Brunton, et. al., "High resolution EUV imaging tools for resist exposure and aerial imaging monitoring", Paper 5751-06 presented at Emerging Lithographic Technologies IX, SPIE, San Jose, CA March 1-3, 2005.

2 High-speed at-wavelength mask inspection

To help qualify the performance of non-actinic inspection tools, a unique dual-mode EUV mask inspection system has been installed at the Advanced Light Source (ALS) synchrotron at Lawrence Berkeley National Laboratory. Capable of both high-speed scanning and defect review imaging, in high-speed inspection mode, whole mask blanks are scanned for defects using 13.5-nm wavelength radiation to identify and map all locations on the mask that scatter a significant amount of EUV light. In imaging (or defect review mode) a zone plate is placed in the reflected beam path to image a region of interest onto a CCD detector with an effective resolution on the mask of 100-nm or better. Combining the capabilities of the two inspection tools into one system provides the unique capability to determine the coordinates of native defects that can be used to compare actinic defect inspection with visible light defect inspection tools under commercial development, and to provide data for comparing scattering models for EUV mask defects. Note that the current intent for this review step is to image the defect using the same imaging properties (e.g. resolution) as the proposed projections optics to be used in EUVL production tools. Higher resolution optics are planned to be installed at later date, but will serve a purpose other than the direct assessment of printability.

To date the highest sensitivity for EUV defect detection (in inspection mode) has been obtained in dark-field mode where only the light scattered out of the entrance pupil is detected[4]. There is background scatter from the multilayer of the order of 0.5% to 1% above which the dark-field signal from a defect must rise in order to be registered as a defect – and this sets a theoretical bound on the signal to noise ratio obtainable in dark-field imaging mode. Signal-to-noise improves as the scanning spot size is decreased, at the expense of reduced flux and more points required to scan a complete mask. Our analyses of the trade-off between scan speed, beamline flux and signal to noise levels for this system indicates an optimum point with a 1μm spot size on the mask. Dark-field imaging is insensitive to absorption-only defects, therefore we include the capacity for simultaneous bright-field and dark-field detection in scanning (inspection) mode. All data is collected in real time and saved for later analysis.

In order to obtain sufficient statistics to determine whether visible light scattering tools are seeing all relevant multilayer defects, it is necessary to scan several hundred square centimetres of mask blank. The capacity for high-speed, continuous operation of the tool over large areas of mask surface is therefore critical. Speed is essential as the defect density is anticipated to be low – of the order of 0.05 defects/cm^2 or one defect in every 20cm^2 (on average).

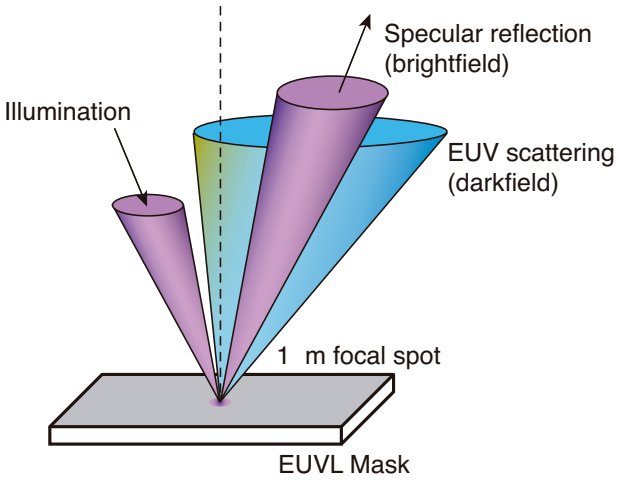

Figure 2
Dark-field scattering is used to locate multilayer defects on the mask.

[4] "Actinic EUVL mask blank defect inspection system", S. Jeong et al, Proc. SPIE Vol. 3676, p. 298-308, 1999; "Actinic detection of multilayer defects on EUV mask blanks using LPP light source and dark-field imaging" Y.Tezuka et.al. Proc. SPIE Vol. 5374, p. 271 (2004).

The conceptual layout of the system is illustrated below. EUV light from ALS beamline 11.3.2 is focused on a pinhole, which is re-imaged onto the mask using Schwarzschild optics with a demagnification factor of 20x. All multilayer mirrors have been wavelength matched through the system. Peak throughput of the system is at 13.4nm, and masks must be matched to this wavelength in order to achieve optimum system throughput and sensitivity.

The EUV light incident into a 1µm spot on the mask has been measured to be of 1.3µW of in-bad EUV light centred on 13.4nm with the bandpass at 230mA ALS current using a 20µm pinhole upstream of the Schwarzschild optics. The diode response in known to be 0.12A/W at EUV wavelengths, giving an incident flux on the mask. This is well within specifications for achieving the target $2cm^2$/hr scan speed of the mask scanner in high-speed scanning mode. Higher flux can be achieved using larger pinholes and/or slits at the expense of a larger illuminated area, resulting in lower sensitivity to small defects.

Masks are rotated and translated under the illuminated spot to produce annular scan sections, with sufficient translation to scan the entire surface area of standard 6" square mask blanks. Because of space constraints between the Schwarzschild optic and the mask it difficult to put detectors in this location; instead, we use a scraper mirror to reflect the scattered light to the side where the brightfield signal is captured on a photodiode and the darkfield signal is registered on a channelplate.

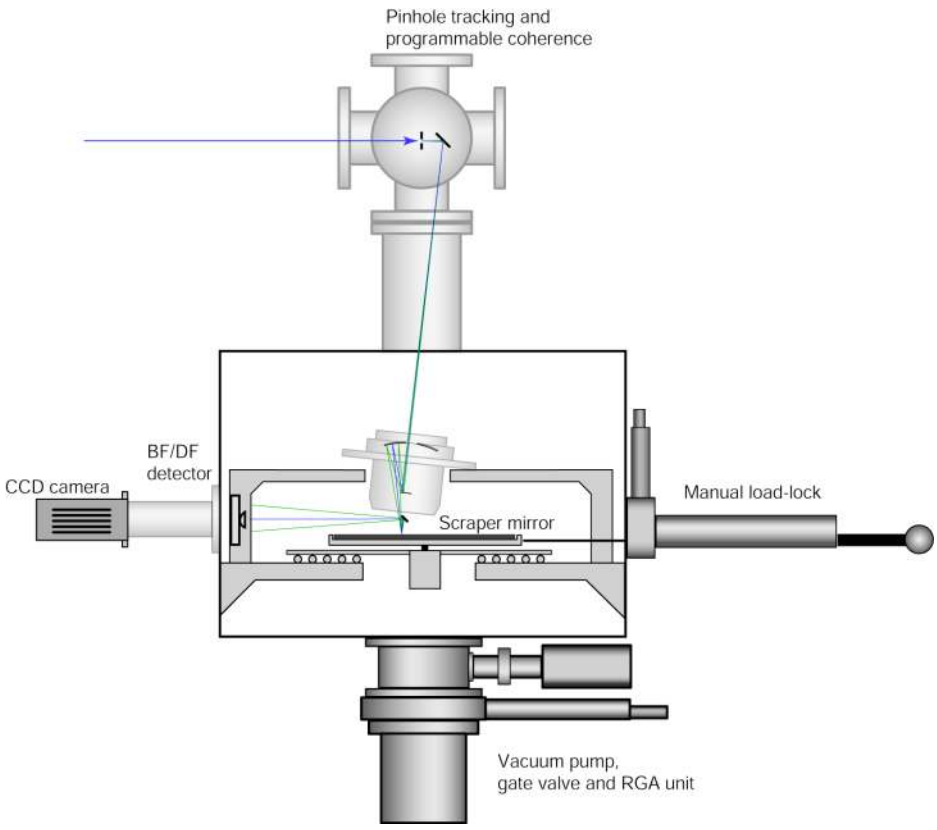

Figure 3

Conceptual layout of the scanning system design. A 1µm spot is produced by re-imaging a 20µm pinhole onto the mask using Schwarzschild optics with a demagnification factor of 20x. Because of space constraints between the Schwarzschild optic and the mask, it difficult to put detectors in this location; instead, we use a scraper mirror to reflect the scattered light to the side where the brightfield signal is captured on a photodiode and the darkfield signal is registered on a channelplate.

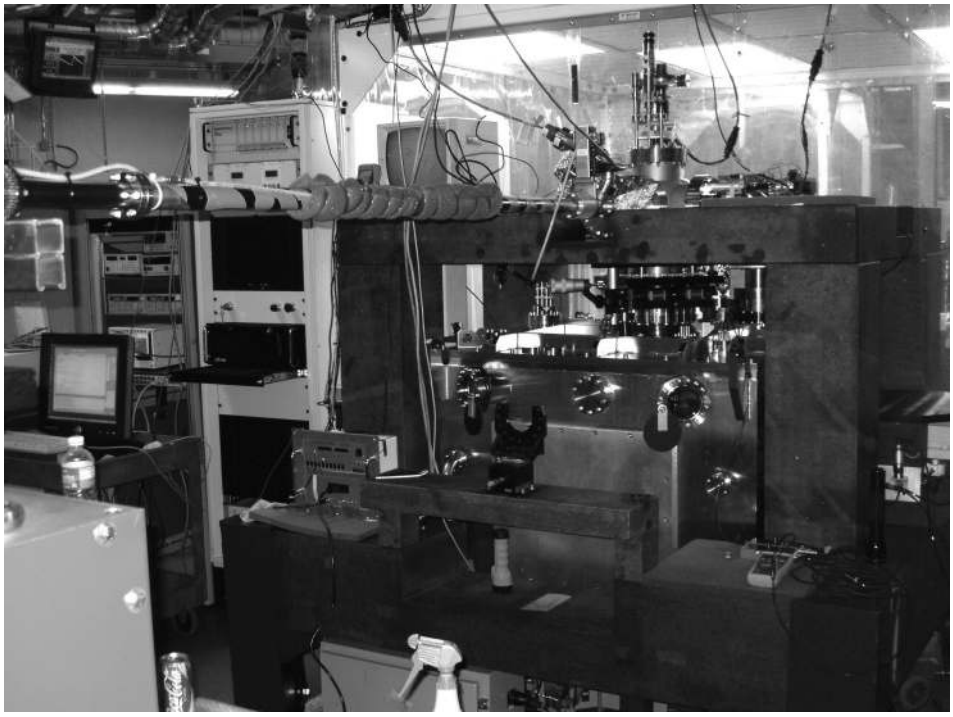

Figure 4
The actinic mask inspection system installed at beamline 11.3.2 at the Advanced Light Source, Berkeley.

All data is saved in real time, enabling subsequent review and analysis of defect signatures. Coordinate transfer between the actinic inspection system and other defect review tools is performed via fiducial markers, enabling defect signatures to be compared between inspection systems. Once detected in scanning mode, defects can subsequently be imaged in review mode using the inbuilt at-wavelength zone plate imaging microscope.

3 Test samples

Experiments are underway using both programmed defect mask blanks and low-defect mask blanks drawn from existing mask pilot lines. Both types of sample have inherent advantages and disadvantages for inspection cross-correlation experiments:

1. Programmed defects: involve artificially generating known defect structures believed to be representative of the types of defects found on production masks. Scanning for the defects can be made comparatively efficient if the defect density can be made comparatively high and the defect locations can be known in advance. The fact that all of the defects are nominally identical means that it is possible to generate good statistics on a given class of defect, whilst arranging the defects in a regular structure enables false counts to be easily discarded.

   This is particularly useful if the programmed defect structures are selected to be at or near the detection threshold of a given tool for scanning sensitivity analysis. Furthermore, the use of controlled programmed defects allows for cross-comparison with the results of printing experiments using patterned masks on programmed defect substrates.

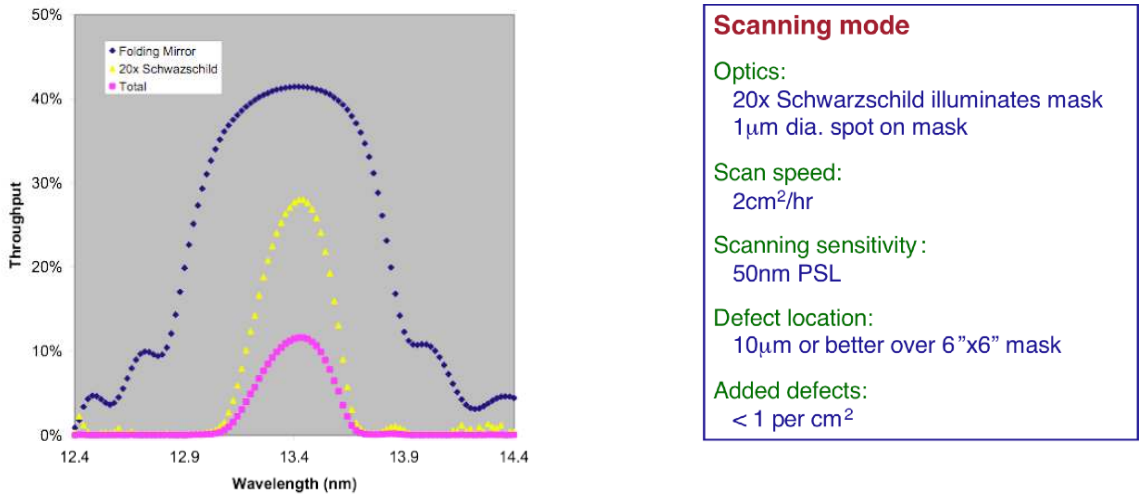

Figure 5
Wavelength response of the reassembled end-station as measured after the illumination optics and after installation. Peak throughput is at 13.4nm.

The downside of using programmed defects is that the defect distribution is by definition not representative of the defect distribution on a production mask, thus programmed defects are not suitable for generating data on the frequency with which different defect types can be expected on a real mask blank. Furthermore using programmed defects requires the most difficult-to-find class of defects to be anticipated and then fabricated, and precisely which defects fall into this class may not be known until pilot production lines are established, and they may differ among mask suppliers.

2. Native defects: involve inspecting mask blanks manufactured in a production environment. The defect density will be comparatively low, however the defect population statistics will represent that of the production environment and will therefore yield cross-correlation data representative of production masks. A clear advantage is that the samples are easy to make, as no special effort is required to produce 'programmed' defects. However, there are also disadvantages to using native defect samples. With a low anticipated defect density, large areas of mask must be inspected in order to gather adequate statistics, and no fundamental knowledge is gained on what makes a particular defect visible in either the actinic or non-actinic inspection tool. Furthermore native defect studies sample a population of defects specific to one deposition process. It can not be guaranteed that the statistics of this population will remain constant as deposition processes evolve, therefore one would have to expect to repeat studies of native defect populations as multilayer deposition technology evolves.

The use of both programmed defect and native defect samples provides complementary information on defect inspection capability: programmed defect samples can be used to provide in-depth learning on defect printability and defect detection sensitivity in both the actinic and non-actinic inspection tools, whilst the study of production mask blanks provides statistical data on defect types and levels in masks manufactured in a production environment.

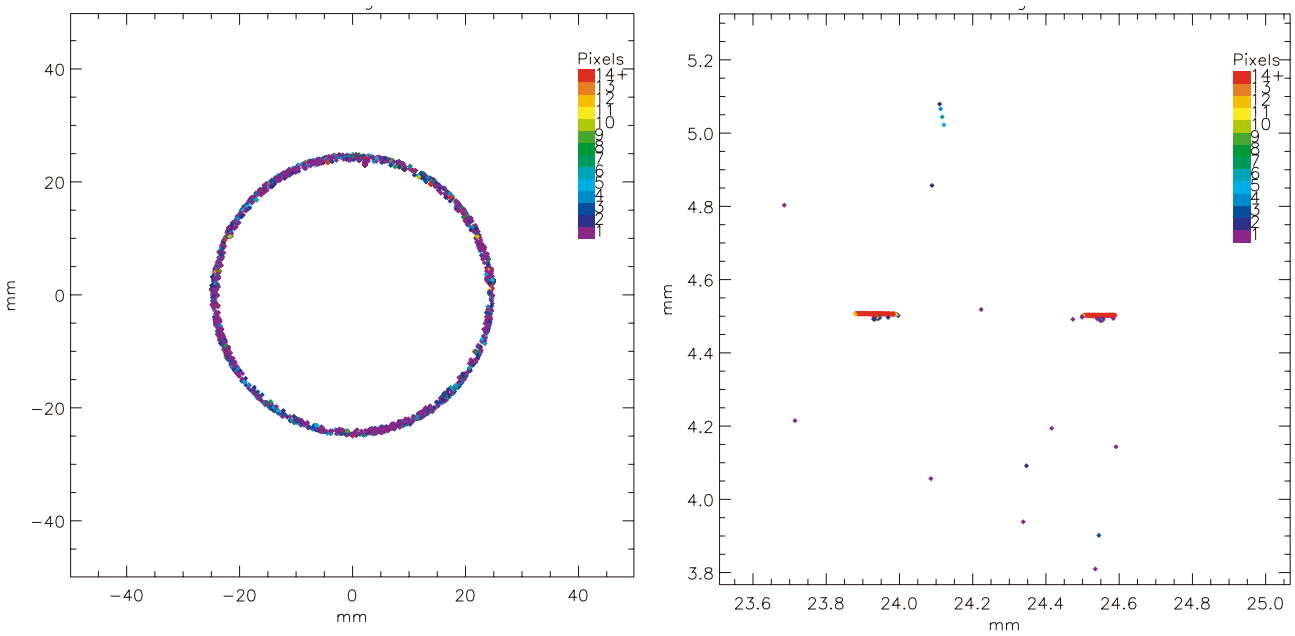

Figure 6

A typical annular scan pattern (left) from one data measurement run, in this case on a high-defect mask to illustrate the shape of the scan pattern. Co-ordinates are relative to the mask centre. On the right is a 1.5x1.5mm detailed region of the same scan pattern, as indicated by the length scale on the axes. This scan clearly shows two fiducial markers patterned underneath the reflective multilayer coating along with several native defects. In these plots, colour coding represents the size of the defect, being the number of successive data 'pixels' during which the signal was above detection threshold.

4 First data from the inspection system

The at-wavelength mask inspection system was installed at the ALS during October 2004, with first results and calibration being performed from November 2004 through to February 2005. Figure 4 shows the new inspection end-station installed at the ALS, and Figure 5 shows the measured wavelength response of the system as installed. To ensure maximum throughput masks should be wavelength matched to the fixed wavelength response of the inspection system.

A typical annular scan pattern is shown in Figure 6. The left panel shows data from one data measurement run, intentionally performed on a high-defect mask for system calibration and to illustrate the shape of the scan pattern. Co-ordinates are relative to the mask centre. On the right is a 1.5x1.5mm^2 detailed region of the same scan pattern, as indicated by the length scale on the axes. This scan clearly shows two fiducuial markers patterned underneath the reflective multilayer coating along with several native defects. In these plots, color coding represents the size of the defect, being the number of successive data 'pixels' during which the signal was above detection threshold. Inspection of large areas of mask blank is possible - in a recent data run (not shown) 80cm^2 were scanned in a time of 40 hours.

Whilst the scan is in progress, all data is saved to disk in real time, enabling subsequent analysis and review of the defect inspection signals. One interesting observation is that some defects are observed to occur in either the brightfield or darkfield channels, but not both, whilst other defects appear in both channels. This is illustrated by the line-out traces in Figure 7 taken from a selection of native defects. Note that in some cases there is a distinct change in darkfield signal, but very little change in brightfield signal, whereas in other cases there is a change in only the brightfield channel but not the darkfield channel. In yet other cases, a clear signal is seen in both the bright- and dark-field channels of the inspection system. These results are from initial data and the root cause of the differences has not yet been determined.

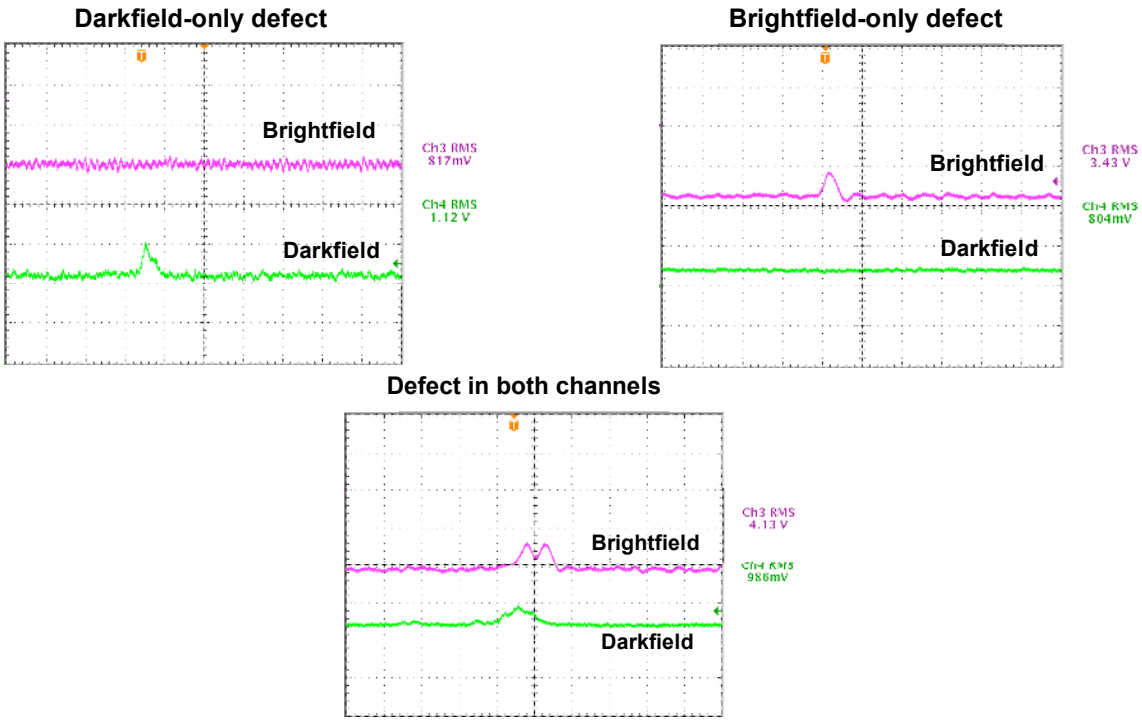

Figure 7

A selection of measured signals from native defects. Some defects are observed to occur in either the brightfield or darkfield channels, but not both, whilst other defects appear in both channels. Determining the cause of these differences, and its impact on both defect printability and inspection in commercial inspection tools, is a key goal of this project.

Analyzing and understanding the cause of these differences in at-wavelength inspection signal, and its impact on both defect printability and inspection in commercial inspection tools, is a key goal of this project. This effort is accompanied by numerical calculations designed to model both the defect scattering and optical systems of both actinic, non-actinic and defect printing systems to understand the signals generated for both the brightfield and darkfield detectors and ultimately to predict the comparison in signals between actinic and non-actinic tools.

5 Summary

Sematech has sponsored the installation of a new at-wavelength mask inspection system at beamline 11.3.2 at the Advanced Light Source (ALS), Berkeley. This dual-mode mask inspection system is capable of both high-speed inspection of large areas of mask blank, and defect review using a full-field at-wavelength zone plate microscope designed to emulate the mask-side imaging conditions of the first production stepper systems. Combining the capabilities of the two inspection tools into one system provides the unique capability to determine the coordinates of native defects that can be used to compare actinic defect inspection with visible light defect inspection tools under commercial development, and to provide data for comparing scattering models for EUV mask defects.

This work was performed under the auspices of the U. S. Department of Energy by University of California, Lawrence Livermore National Laboratory under contract No. W-7405-Eng-48.